Springer

KSME

Journal of Mechanical Science and Technology 30 (1) (2016) 1~14
www.springerlink.com/content/1738-494x(Print)/1976-3824(Online)
DOI 10.1007/s12206-015-1201-z

Influence of flexibilities of cranes structural components on load trajectory †

Arkadiusz Trąbka*

Faculty of Mechanical Engineering and Computer Science, Department of Engineering Fundamentals, University of Bielsko-Biala, ul. Willowa 2, 43-309 Bielsko-Biała, Poland

(Manuscript Received November 24, 2014; Revised June 8, 2015; Accepted September 10, 2015)

Abstract

Building computational models of cranes requires using of simplifications. Frequently accepted simplification is ignoring deformations of structural components. At the same time there is no appropriate study concerning estimation of the influence of flexible crane components on the movement of a load. In the paper, the influence of flexibilities of seven crane structural components on working accuracy in relation to the trajectory of the load has been estimated. Numerically efficient telescopic crane model has been developed with the use of the finite element method. Beside of qualitative analysis used in other works to evaluate the results, a method of quantitative analysis proposed by the author has been applied. The analyses show that based on computational models one can make proper assessment of a load motion. The condition is a proper selection of considered flexible components. A parametric identification and/or quantitative assessment should be a criterion of models configuration.

Keywords: Crane structural components; Finite element method; Load movement; Quantitative analysis; Rigidity/flexibility; Working accuracy

1. Introduction

Cranes are hoisting devices that take many different forms of structure. Diversity of types and dimensions enables that, they are able to perform all works of reloading, loading and unloading in almost all conditions. For the work to be efficient and performed with high precision, numerous activities are carried out to improve operational parameters of cranes. Therefore, both existing and currently designed cranes are submitted for numerical analysis. Unfortunately, the analyses are frequently made without adequate care in relation to reproducing dynamic characteristics of real structures in numerical models. Of particular importance for the abovementioned problem are flexibilities of crane structural components. Flexible components are included in computational models in varying numbers but without justification of selection criteria.

Computational crane models composed of components treated as non-deformable and one flexible component were used in Refs. [1-5]. Models with an increased number of flexible components to two were used in Refs. [6-9]. In Refs. [10-16] for slewing motion the number of flexible components was increased to three. In Refs. [16-18] for lifting motion four flexible components were used in addition to non-deformable components. Models made of non-deformable components and five flexible components were used in Refs. [19-21]. Models containing only flexible components were used in Refs. [22-25]. Among numerous scientific papers concerning cranes one can also find those in which computational models were completely deprived of flexible components [26-33].

Computational crane models differ not only in the number of flexible components taken into account, but also in the number of components considered as non-deformable. There are also differences in selection of the components used for building models. Therefore, cranes with similar or even identical structure are analysed on the basis of completely different models. For example, in Ref. [6] the flexibilities of a tower and a jib were taken into account in a tower crane model. At the same time a rope hoisting system and drives were treated as non-deformable. On the other hand, in Ref. [28] a simple system model consisting only of rigid components, i.e. a jib, a rope and a load was adopted for the analysis of the same kind. In this model the input was implemented in the form of the jib rotation directly in the joint between the jib and the tower.

Similar cases of differences between the models are present in papers concerning floating cranes [3-5, 18, 22, 24, 26, 29, 30].

Due to the complexity of the structure, much greater differences between the models can be seen in papers concerning the analysis of dynamic properties of cranes with telescopic booms [2, 7, 10-17, 19-21]. For example, in Ref. [10] the slewing motion of a crane body was analysed by means of a model which assumed a non-deformable crane frame rigidly

*Corresponding author. Tel.: +48 338279226, Fax.: +48 338279226
E-mail address: atrabka@ath.bielsko.pl
† Recommended by Editor Yeon June Kang

connected with the ground, a non-deformable slewing platform, a non-deformable luffing hydraulic cylinder and an inextensible hoisting rope. However, bending flexibility of a three-member boom, flexibility of slide blocks and a drive were taken into account. The model, which was used in Ref. [14], assumed the following components as rigid: a support frame, a slewing platform, a slewing motion drive and a boom. For the boom, its substitute flexibility was taken into account by introducing a torsion spring in the joint which connects it to the platform. Spring-damper elements were also used to model the flexibilities of outriggers and a rope.

Authors of models do not usually justify the selection criteria. They limit themselves to sporadic verifying the obtained results by comparing them with the study results. Tests are frequently performed not on real objects but on specially built laboratory models. Examples of this approach may be found in Refs. [12, 17, 19, 23, 29, 33]. Sometimes verification boils down to performing analogous calculations using the model developed by means of another numerical method, such as in Ref. [18].

In only a few cases, the authors of papers attempted to justify the need to take into account the flexibility of selected structural components in computational models of cranes. For example, in Ref. [16] the luffing hydraulic cylinder was the subject of such considerations, in Refs. [2, 17] the outriggers, in Refs. [3, 5] the boom.

One of a few attempts to comprehensive estimate the influence of the flexibility of components on dynamic properties of a crane model was performed by Jerman and Kramar in Ref. [27]. On the basis of an earlier developed mathematical model of a tower crane which consisted only of flexible components [23], neglecting deformability of the structure and energy dissipation, the authors compared the forces which act on the model in the horizontal plane with the results of a real crane tests, which allowed estimating the influence of the flexibility of crane components on the determined forces.

A similar task as the one by Jerman and Kramar, but in relation to a telescopic crane model, was undertaken by Mijailović in Ref. [21]. He took into account the flexibility of five crane components, i.e. outriggers, a support frame, a slewing bearing, a luffing hydraulic cylinder and a boom. As a result of the analyses he determined the amount of errors that is caused by not taking into account flexibility of individual components in the analyses of dynamic properties of cranes with telescopic booms.

None of the found papers undertakes an analysis evaluating possible relations between the selection of flexible components, the correctness of working movements and the influence of the selection on the movement of the load.

Because within the scope of above-mentioned subject area an adequate study was not found this paper aims at estimating the influence of flexibilities of crane structural components (especially those frequently neglected) on working accuracy in relation to the trajectory of the load.

To achieve the intended aim among different methods of description of dynamic systems (e.g. Lagrange, Hamilton, multibody systems, finite elements) the Finite element method (FEM) has been selected. This method allowed to develop numerically efficient and at the same time universal computational crane model.

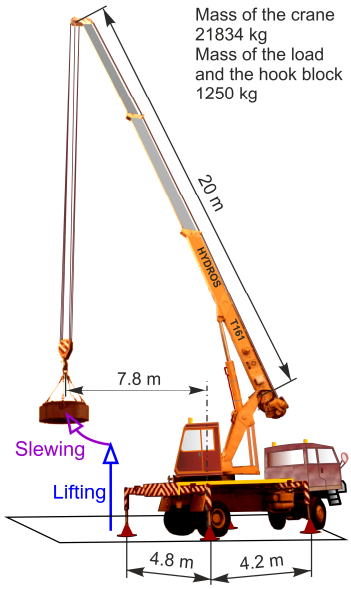

Fig. 1. Real structure of the HYDROS T-161 telescopic crane.

2. Computational model

Among many crane types being analysed, the structure most frequently submitted for numerical analyses has been selected. For the purpose of the tasks carried out in the work a computational model of a so-called telescopic crane, based on the structure of the HYDROS T-161 hydraulic truck crane (Fig. 1) (with a three-member telescopic boom and a displaced axis of rotation), has been developed. This model took into account the flexibilities of until the seven structural components. Four of them, i.e. outriggers, a boom, a rope hoisting system and a luffing hydraulic cylinder, are frequently taken into account in computational models. Among rarely taken into account components, a flexible support frame and flexible elements of a telescopic mechanism, i.e. a hydraulic cylinder and a rope system were used. The model also took into account the flexibility of elements of a boom supporting system, overlooked in the dynamic analyses.

2.1 Physical model

On the basis of the information contained in the design crane documentation and the technical manual documentation a physical model has been developed. This model was obtained as a result of the following simplifying assumptions in relation to the real crane structure [34]:

(1) A car chassis, a slewing platform and a girder were assumed as rigid.

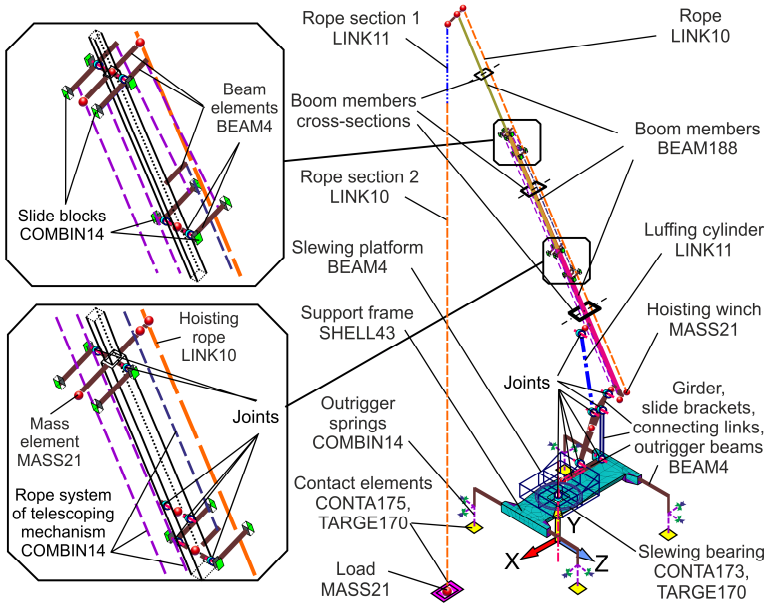

Fig. 2. Discrete model of the HYDROS T-161 telescopic crane.

(2) All joints between parts were taken into account but clearances and friction were omitted.

(3) The boom was modelled as a system of three flexible beams connected by means of slide blocks with the geometry consistent with the design documentation.

(4) The masses of most of the parts mounted on the boom as well as the masses of the outriggers were taken into account.

(5) The masses of hydraulic equipment parts were taken into account as well as the change in mass distribution caused by motion for the hydraulic cylinder.

(6) The load and a hook block were assumed in the form of material points.

(7) The possibility of the outriggers and the load detachment from the ground was taken into account.

2.2 Discrete model

On the basis of the physical model a discrete model of the crane has been built (Fig. 2). This model was developed with the use of the FEM method and saved using the ANSYS parametric design language (APDL) in the ANSYS software [35] (APDL is a set of commands used to construct the model in Notepad without a Graphical user interface).

For discretisation only finite elements were used allowing to take into account geometric nonlinearities such as large strains and large rotations.

Large strains were calculated using an incremental solution procedure in accordance to the relation:

$$\boldsymbol{\varepsilon}_n = \boldsymbol{\varepsilon}_{n-1} + \Delta\boldsymbol{\varepsilon}_n \tag{1}$$

where $\boldsymbol{\varepsilon}_n$ is the total Hencky strain tensor at the time step n, $\boldsymbol{\varepsilon}_{n-1}$ is the total Hencky strain tensor at the previous time step n-1, $\Delta\boldsymbol{\varepsilon}_n$ is the strain increment tensor.

The details about calculations of large strains are presented in Appendix A.1.

Large rotations were analysed by means of a transformation matrix $\mathbf{T}_\omega$ associated with a rotational pseudovector.

$$\mathbf{T}_\omega = \mathbf{I} + \sqrt{1-\left(\frac{\omega}{2}\right)^2}\cdot\boldsymbol{\Omega} + \frac{1}{2}\cdot\boldsymbol{\Omega}^2 \tag{2}$$

where $\mathbf{I}$ is the identity matrix, ω is the length of the rotational pseudovector and $\boldsymbol{\Omega}$ is the pseudovector skew-symmetric matrix representation.

The details about the above matrix and its relationship with the rotational pseudovector are shown in Appendix A.2.

2.3 Description of the dynamic system

The dynamic system taken into consideration in the work describes the equation of motion of a form:

$$\mathbf{M}\cdot\frac{d^2\mathbf{u}}{dt^2} + \mathbf{K}\cdot\mathbf{u} = \mathbf{F} \tag{3}$$

where $\mathbf{M}$ is the structural mass matrix, $\mathbf{K}$ is the structural stiffness matrix, $\frac{d^2\mathbf{u}}{dt^2}$ is the nodal acceleration vector, $\mathbf{u}$ is the nodal displacement vector, $\mathbf{F}$ is the applied load vector.

The Newmark time integration method was used for the solution of Eq. (3). This method uses finite difference expansions in a time interval Δt. Eq. (3) is evaluated at time $t+\Delta t$ as:

$$\mathbf{M}\cdot\left.\frac{d^2\mathbf{u}}{dt^2}\right|_{(t+\Delta t)} + \mathbf{K}\cdot\mathbf{u}_{(t+\Delta t)} = \mathbf{F}_{(t+\Delta t)}. \tag{4}$$

The Newmark equations are as follows:

$$\left.\frac{d\mathbf{u}}{dt}\right|_{(t+\Delta t)} = \left.\frac{d\mathbf{u}}{dt}\right|_{(t)} + \left[(1-\delta)\cdot \left.\frac{d^2\mathbf{u}}{dt^2}\right|_{(t)} + \delta\cdot \left.\frac{d^2\mathbf{u}}{dt^2}\right|_{(t+\Delta t)}\right]\cdot\Delta t \tag{5}$$

$$\mathbf{u}_{(t+\Delta t)} = \mathbf{u}_{(t)} + \left.\frac{d\mathbf{u}}{dt}\right|_{(t)}\cdot\Delta t + (\Delta t)^2\cdot\left[\left(\frac{1}{2}-\alpha\right)\cdot\left.\frac{d^2\mathbf{u}}{dt^2}\right|_{(t)} + \alpha\cdot\left.\frac{d^2\mathbf{u}}{dt^2}\right|_{(t+\Delta t)}\right] \tag{6}$$

where α and δ are the Newmark integration parameters.

Solving Eq. (6) relative to the second derivative of the displacement vector $\mathbf{u}$ for time $t+\Delta t$ and substituting the calculated value into Eq. (5), Eqs. (7) and (8) are obtained.

$$\left.\frac{d\mathbf{u}}{dt}\right|_{(t+\Delta t)} = \frac{\delta}{\alpha\cdot\Delta t}\cdot(\mathbf{u}_{(t+\Delta t)}-\mathbf{u}_{(t)}) + \left(1-\frac{\delta}{\alpha}\right)\cdot\left.\frac{d\mathbf{u}}{dt}\right|_{(t)} + \Delta t\cdot\left(1-\frac{\delta}{2\cdot\alpha}\right)\cdot\left.\frac{d^2\mathbf{u}}{dt^2}\right|_{(t)} \tag{7}$$

$$\left.\frac{d^2\mathbf{u}}{dt^2}\right|_{(t+\Delta t)} = \frac{1}{\alpha\cdot(\Delta t)^2}\cdot\left[\mathbf{u}_{(t+\Delta t)}-\mathbf{u}_{(t)} - \left.\frac{d\mathbf{u}}{dt}\right|_{(t)}\cdot\Delta t - (\Delta t)^2\cdot\left(\frac{1}{2}-\alpha\right)\cdot\left.\frac{d^2\mathbf{u}}{dt^2}\right|_{(t)}\right]. \tag{8}$$

Substituting Eq. (8) into Eq. (4) we obtain:

$$\left[\frac{1}{\alpha\cdot(\Delta t)^2}\cdot\mathbf{M}+\mathbf{K}\right]\cdot\mathbf{u}_{(t+\Delta t)} = \mathbf{F}_{(t+\Delta t)} + \mathbf{M}\cdot\left[\frac{1}{\alpha\cdot(\Delta t)^2}\cdot\mathbf{u}_{(t)} + \frac{1}{\alpha\cdot\Delta t}\cdot\left.\frac{d\mathbf{u}}{dt}\right|_{(t)} + \left(\frac{1}{2\cdot\alpha}-1\right)\cdot\left.\frac{d^2\mathbf{u}}{dt^2}\right|_{(t)}\right]. \tag{9}$$

The resulting equation allows to determine the displacement vector $\mathbf{u}$ for time $t+\Delta t$. The velocity and acceleration vectors are calculated from Eqs. (7) and (8).

The Newmark method is unconditionally stable for the parameters α and δ selected on the basis of conditions Eq. (10) [36].

$$\delta \geq 0.5\,,\quad \alpha \geq 0.25\cdot(\delta+0.5)^2\,,\quad \alpha+\delta+0.5>0\,. \tag{10}$$

Eq. (9), due to its non-linearity, at each time step is solved iteratively using the Newton – Raphson method [37].

By repeating the procedure outlined above for the next time steps we obtain a solution in the considered time interval.

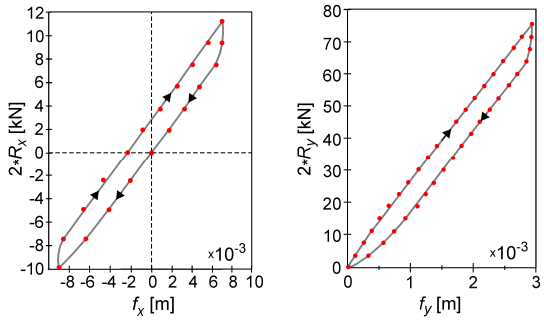

(a) (b)

Fig. 3. Force - displacement dependences obtained on the basis of the HYDROS T-161 crane studies (described in Ref. [41]) for the rear pair of outriggers: (a) in horizontal plane; (b) in vertical direction.

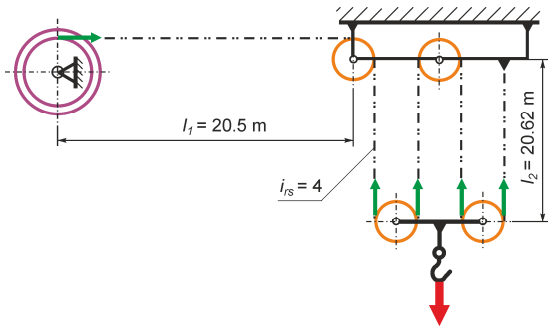

Fig. 4. Diagram of the hoisting rope system.

2.4 Model parameters

The dimensions of the model, the cross-sections of particular crane components and their material parameters were specified based on the design of the HYDROS T-161 crane.

The stiffnesses of the outriggers, the support frame, the boom, the boom supporting system elements and the hoisting rope system were based on the research results of this crane, described in Ref. [38].

For the outriggers, based on the shapes of the characteristics shown in Fig. 3, linear dependences of forces on displacements were adopted as admissible [38]. For each outrigger, the average stiffnesses: $k_x = 0.6\text{E}6$ N/m, $k_z = 0.6\text{E}6$ N/m, $k_y = 12.5\text{E}6$ N/m were determined.

For the hoisting rope system (Fig. 4), according to dependence Eq. (11) whose derivation is shown in Ref. [38], a substitute stiffness $k_r = 13.33\text{E}6$ N/m was determined. The average stiffness per length unit $k_{ru} = 85.75\text{E}6$ (N/m)/m was applied in calculations. The choice of the average as a value properly characterising the unit stiffness was based on the results of the tests of a rope test section performed on a testing machine.

$$k_r = \frac{k_{ru}\cdot i_{rs}^2}{l_1 + i_{rs}\cdot l_2} \tag{11}$$

where k_{ru} is the rope unit stiffness, i_{rs} is the number of the rope strands in the sheave block, l_1 is the distance between

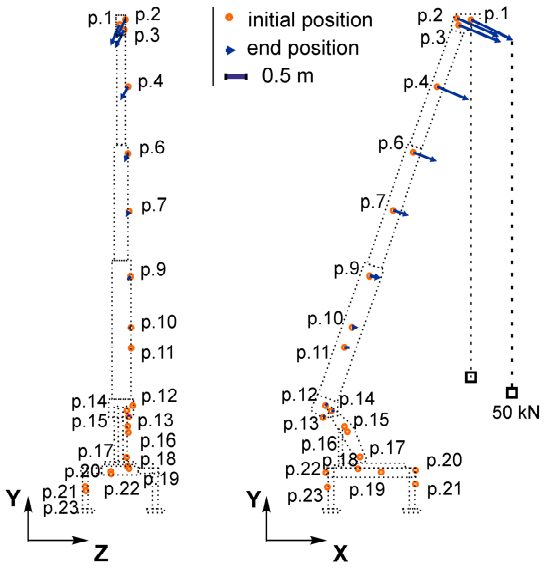

Fig. 5. Displacements of measuring points marked on the boom, the boom supporting system and the support frame, presented in YZ and YX planes (direction designations as shown in Fig. 2).

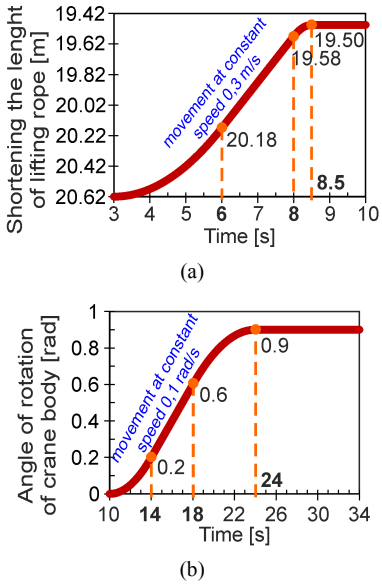

Fig. 6. Kinematic input functions: (a) lifting of the load; (b) rotation of the crane body.

the hoisting winch and the boom head, l_2 is the distance between the hook block and the boom head (see Fig. 4).

For the boom modelled as a system of flexible beams it was assumed that there is a compatibility of displacements of selected points on the model of the boom and the real object (the masses and the mass moments of inertia for the particular boom components as well as the stiffnesses of slide blocks were chosen according to the above assumptions). The same approach was applied for the model of the support frame and the elements of the boom supporting system. All comparisons were made with reference to the results of measurements made with a photogrammetric method [38] for the real crane structure. Examples of the results of these measurements are shown in Fig. 5.

The stiffnesses of the luffing hydraulic cylinder and the telescopic cylinder, due to the lack of access to research results, were based on the data taken from Refs. [39, 40]. Following the authors of the above-mentioned works the average stiffnesses of hydraulic cylinders were assumed respectively: k_{lhc} = 5E7 N/m for the luffing hydraulic cylinder and k_{tc} = 1.6E6 N/m for the telescopic hydraulic cylinder.

3. Numerical analysis of the model

The analysis concerned the model of the crane with a completely extended boom (a length of 20 m), inclined at an angle of 60° (a crane radius of 7.8 m). A load of 1000 kg was adopted. Kinematic input functions were used for the drive of various crane mechanisms (Figs. 6(a) and (b)).

3.1 Assumptions for the calculations

The crane model was prepared for the calculations assuming that the clearances and friction in drives as well as flexibilities of joints and damping in the system are not taken into account. Additionally it was assumed that the outriggers rest on the rigid ground and the influence of external factors (e.g. wind pressure) on the crane components or the load is neglected. A variable step of integration in the range of 0.001 to 0.0001 s was adopted.

3.2 Numerical simulations

Numerical simulations were carried out for a sequence of working movements of lifting and slewing. In subsequent stages of the analysis the following were considered:

(1) Bringing the crane to a state of static equilibrium.

(2) Tensioning the rope up to the moment of separation of the load from the ground.

(3) Lifting the load after separation from the ground.

(4) Rotation of the crane body relative to the chassis after discontinuing of lifting.

(5) Free movement of the load after stopping the slewing motion.

As a reference model for the numerical simulations a system (consisting of 370 nodes and 335 finite elements) was adopted, where all components were treated as non-deformable. This model was referred to as "a rigid model". As a result of substituting the following non-deformable components with flexible components in the rigid model, seven crane model variants were obtained, each containing one flexible component. As the final variant of the system the connection of flexible components into one structure was adopted. The resulting system (consisting of 1739 nodes and 1865 finite elements) was called "a flexible model".

Table 1. Variants of telescopic crane model.

Crane components	V1	V2	V3	V4	V5	V6	V7	V8	V9
Hoisting rope system	N	**F**	N	N	N	N	N	N	**F**
Outriggers	N	N	**F**	N	N	N	N	N	**F**
Support frame	N	N	N	**F**	N	N	N	N	**F**
Elements of telescopic mechanism	N	N	N	N	**F**	N	N	N	**F**
Elements of boom supporting system	N	N	N	N	N	**F**	N	N	**F**
Luffing hydraulic cylinder	N	N	N	N	N	N	**F**	N	**F**
Boom	N	N	N	N	N	N	N	**F**	**F**

F – Designation of component assumed in a given variant of the crane model as flexible;
N – Designation of component assumed in a given variant of the crane model as non-deformable.

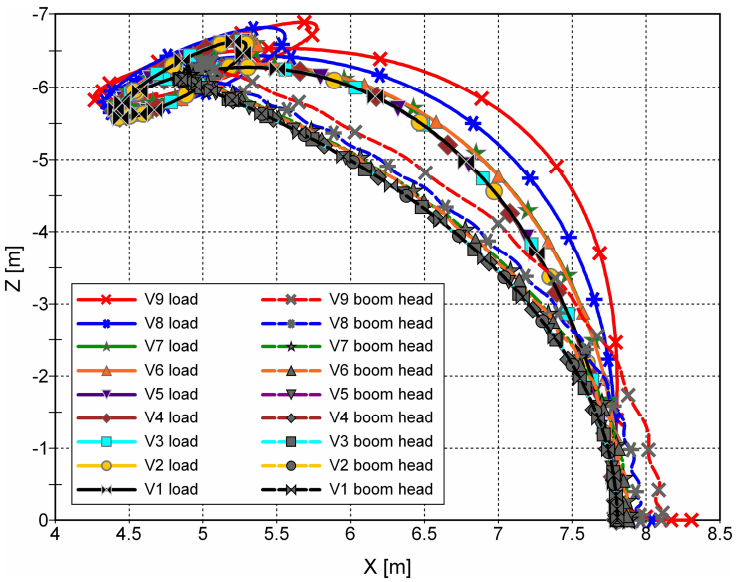

Fig. 7. Trajectories of the load and the boom head during rotation (visible in the plane of rotation), for variants V1-V9.

Variants of telescopic crane model for which numerical simulations were performed are summarised in Table 1.

3.3 Results analysis

The influence of the model components flexibility on the accuracy of the crane work was analysed on the basis of the load trajectory (Figs. 7 and 8) and time characteristics representing horizontal (radial) and vertical components of load positions during rotation of the crane body (Figs. 9(a) and (b)). Due to a close relationship between the load movement and the location of its suspension the trajectories of the boom head (Fig. 7) and the time characteristics of the head displacements during lifting and rotation were also analysed for each variant of the model (Figs. 11 and 13).

To quantify the influence of the flexibility of the structural components on the load and the boom head movement, the average displacements of the load and the boom head were determined for each variant of the model. The average displacements of the boom head for lifting motion of the load (Figs. 11(a) and 13(a)) were determined in relation to the time interval when the head was moving in harmonic motion (i.e. from about 4 to 10 s). Subsequently, the percentages of averages of individual values obtained for variants V2-V8 were calculated with respect to the average values obtained for the flexible and rigid model. These values are assigned respectively 100% and 0% share. The results are shown in Figs. 10, 12 and 14.

On the basis of the numerical simulation results, it was found that:

(1) The trajectories of the load obtained for the variants taking into account the flexibility of the outriggers, the support frame and the telescopic system are most similar to the results obtained for the rigid model treated as a reference model. However, the components introducing the greatest changes in the trajectory of the load are flexible members of the boom, the luffing hydraulic cylinder and elements of the boom supporting system (Figs. 7 and 8).

(2) The influence of the support frame deformations on the trajectory of the boom head and the load is similar to the one

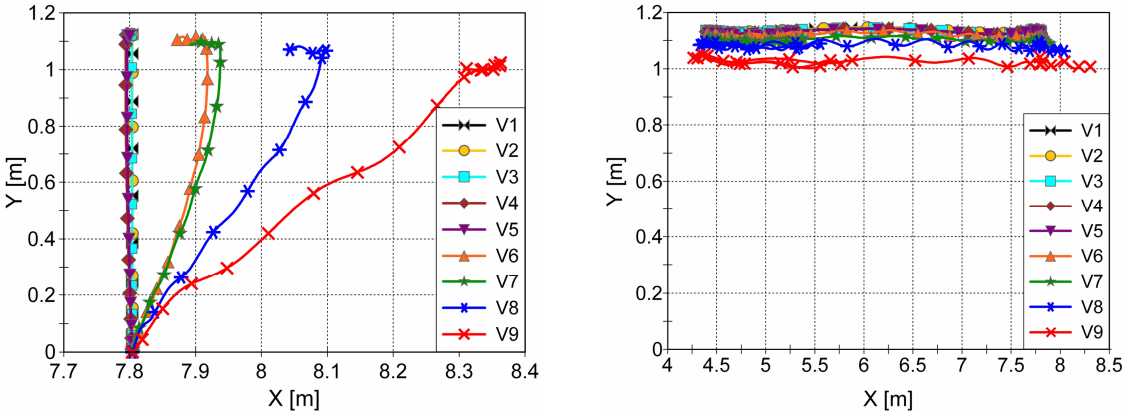

(a) (b)

Fig. 8. Trajectories of the load during: (a) lifting; (b) rotation (visible in the plane of lifting), for variants V1-V9.

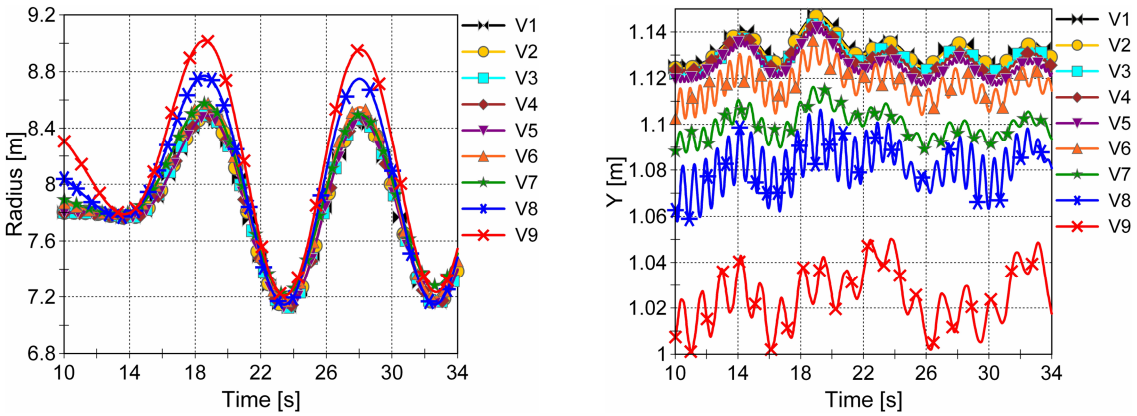

(a) (b)

Fig. 9. (a) Horizontal (radial); (b) vertical components of the load positions during rotation of the crane body, for variants V1-V9.

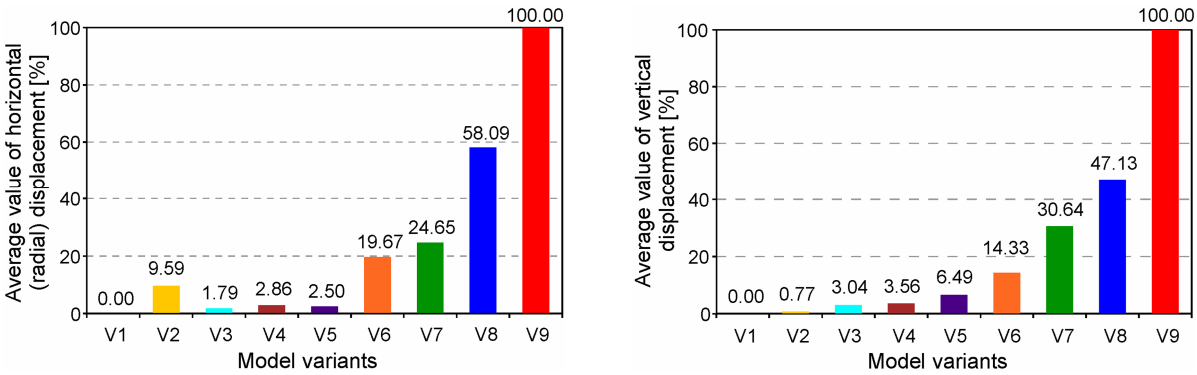

(a) (b)

Fig. 10. Percentage of the average values of: (a) the load horizontal displacements; (b) the load vertical displacements during rotation of the crane body, related to the value obtained for the flexible model: (a) 0.269 m = 100%; (b) 0.108 m = 100%.

caused by deformations of the outriggers.

(3) Despite the fact that the trajectory of the load determined for the model taking into account only the flexibility of the rope system (V2) does not differ in the scale assumed for Fig. 7 from the trajectories obtained for variants V3, V4 and V5, the comparison presented in Fig. 10(a) shows that the average displacement of the load in radial direction is significantly larger for variant V2 than for V3, V4 and V5. The flexibility share of the rope system amounting to 9.59% of the flexibility of the whole system means that this component

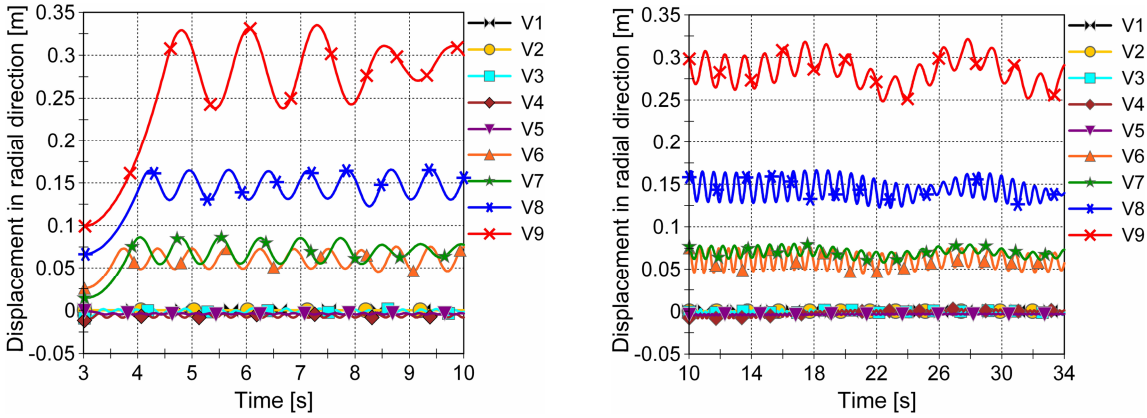

Fig. 11. Horizontal (radial) components of displacements of the boom head during: (a) lifting; (b) rotation, for variants V1-V9.

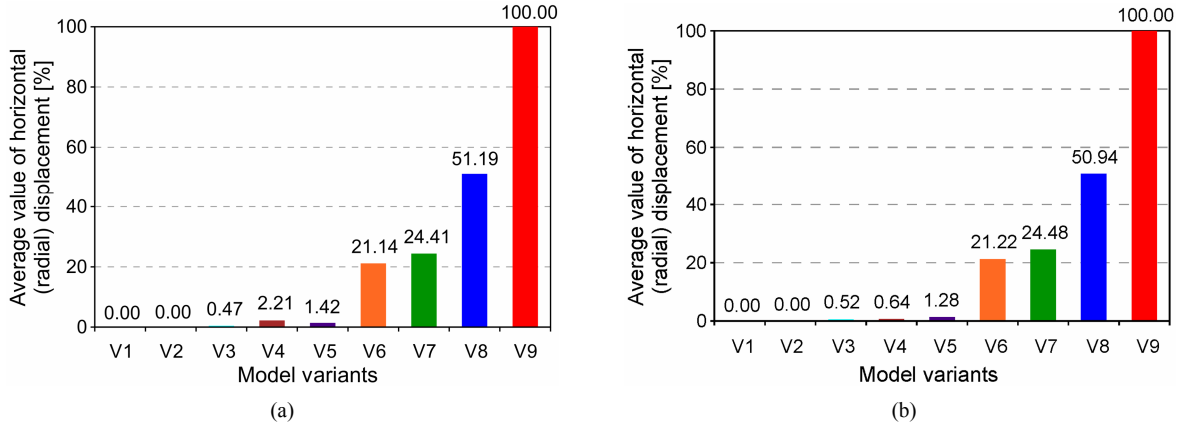

Fig. 12. Percentage of the average values of the boom head horizontal displacements during: (a) lifting of the load; (b) rotation of the crane body, related to the value obtained for the flexible model: (a) 0.287 m = 100%; (b) 0.284 m = 100%.

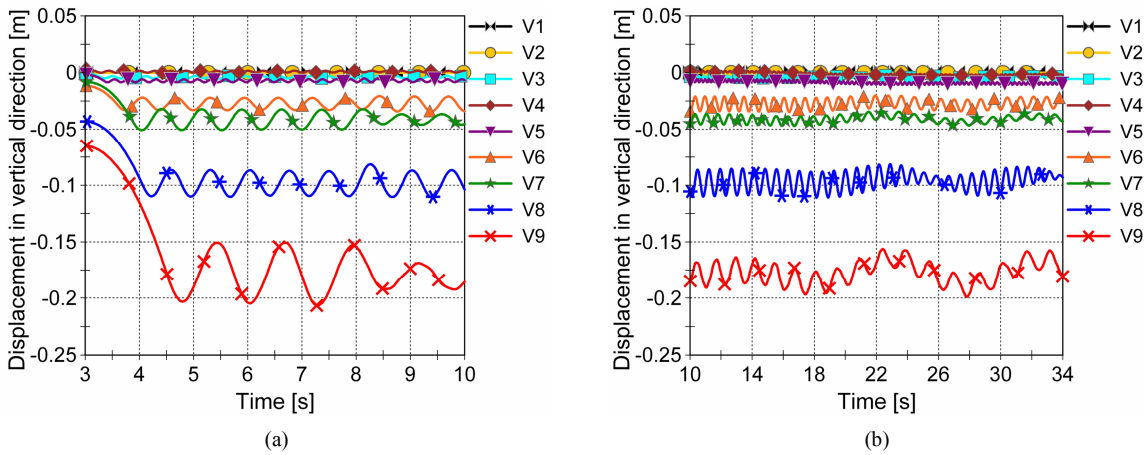

Fig. 13. Vertical components of displacements of the boom head during: (a) lifting; (b) rotation, for variants V1-V9.

flexibility could be taken into account especially during building of the models for analysis of the cranes in a slewing motion.

(4) The time characteristics, which show selected components of the load positions (Fig. 9) and components of the boom head displacements (Figs. 11 and 13), allow to determine whether the flexibility of a particular component contributes to increase or decrease of load swings. In the analysed

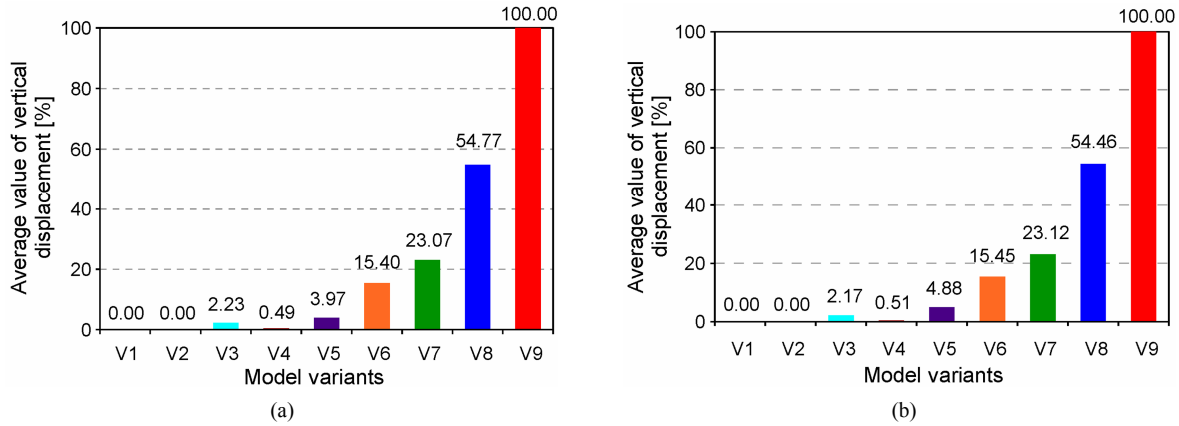

Fig. 14. Percentage of the average values of the boom head vertical displacements during: (a) lifting of the load; (b) rotation of the crane body, related to the value obtained for the flexible model: (a) 0.178 m = 100%; (b) 0.177 m = 100%.

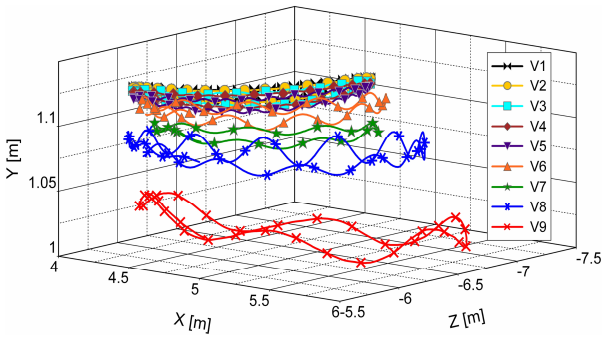

Fig. 15. Trajectories of the load after stopping of slewing motion, for variants V1-V9.

system negative values of components of the boom head horizontal displacements (V3, V4 and V5 in Fig. 11(a)) indicate that the deformations of the outriggers, the support frame and the telescoping system contribute to decrease in the boom head distance from the axis of rotation of the crane body. As a result, the rope angle of deviation from the vertical line decreases at the time of detaching of lifted load from the ground and the load swings are smaller.

4. Conclusions

Seven variants of a telescopic crane computational model, each of which contained one flexible item, were analysed in this paper. The influence of deformations of individual components on the accuracy of a load movement in relation to a rigid and flexible model was examined.

It has been determined that not all components of a telescopic crane structure, despite their finite stiffness, result in significant disturbances in its work. Outriggers, a support frame and a telescoping system are so rigid that in relation to the basic motion carried out by a rigid model, changes of the load trajectory in a slewing motion, taking into account the deformations occurring in these components, are almost imperceptible.

However, on the basis of the numerical analyses, primarily it has been found that:

(1) Deformations that are experienced by components contribute to differences in the load trajectories. These differences are related to a change in the distance of a boom head from the axis of rotation of a crane body as well as to a change in the force of inertia acting on the load during slewing motion.

(2) Magnitude of a load swings which occur after stopping of a slewing motion is closely related to the flexibility of individual structural components of the crane. Swings increase when the flexibilities of the components increase (Fig. 15).

(3) Omitting components with high flexibility in computational models of cranes is unacceptable. Their lack in the models causes adulteration of their dynamic properties. This in turn leads to significant changes in trajectories of loads.

(4) Comparison of time characteristics by means of a quantitative analysis method (as shown in Figs. 10, 12 and 14) enables an unambiguous classification of crane structural components in terms of the influence of their flexibility on the movement of a load (and also the movement of a boom head in telescopic cranes).

(5) One of the most important tasks to be carried out during the development of computational models should be the precise identification of parameters characterising the main structural units of cranes. Properly defined stiffnesses of components will enable the correct choice of those that can be considered as non-deformable. The possibility to neglect their deformations will contribute to improving the numerical efficiency of the models.

Acknowledgements

This work was supported by the Polish Ministry of Science and Higher Education (Grant No. 4 T12C 037 27).

References

[1] S. Kilicaslan, T. Balkan and S. K. Ider, Tipping loads of

mobile cranes with flexible booms, *Journal of Sound and Vibration,* 223 (4) (1999) 645-657.

[2] B. Posiadała, Influence of crane support system on motion of the lifted load, *Mechanism and Machine Theory,* 32 (1) (1997) 9-20.

[3] K. P. Park, J. H. Cha and K. Y. Lee, Dynamic factor analysis considering elastic boom effects in heavy lifting operations, *Ocean Engineering,* 38 (2011) 1100-1113.

[4] J. A. Witz, Parametric excitation of crane loads in moderate sea states, *Ocean Engineering,* 22 (4) (1995) 411-420.

[5] H. L. Ren, X. L. Wang, Y. J. Hu and C. G. Li, Dynamic response analysis of a moored crane-ship with a flexible boom, *Journal of Zhejiang University Science A,* 9 (1) (2008) 26-31.

[6] F. Ju, Y. S. Choo and F. S. Cui, Dynamic response of tower crane induced by the pendulum motion of the payload, *International Journal of Solids and Structures,* 43 (2) (2006) 376-389.

[7] G. Sun and M. Kleeberger, Dynamic responses of hydraulic mobile crane with consideration of the drive system, *Mechanism and Machine Theory,* 38 (2003) 1489-1508.

[8] T. Yoshimoto and Y. Sakawa, Modeling and control of a rotary crane with a flexible joint, *Optimal Control Applications and Methods,* 10 (1989) 21-38.

[9] K. Sato and Y. Sakawa, Modeling and control of a flexible rotary crane, *International Journal of Control,* 48 (5) (1988) 2085-2105.

[10] J. Kłosiński and L. Majewski, Dynamic analysis of a telescopic crane on an automotive chassis, *Proceedings of the 7th World Congress The Theory of Machines and Mechanisms*, Seville, Spain, 3 (1987) 1561-1564.

[11] B. Posiadała and D. Cekus, Discrete model of vibration of truck crane telescopic boom with consideration of the hydraulic cylinder of crane radius change in the rotary plane, *Automation in Construction,* 17 (2008) 245-250.

[12] J. Kłosiński, Swing-free stop control of the slewing motion of a mobile crane, *Control Engineering Practice,* 13 (2005) 451-460.

[13] Z. Towarek, Dynamic of a crane on a soil foundation as a function of the carrier force, *Machine Vibration,* 5 (1996) 211-223.

[14] Z. Towarek, The dynamic stability of a crane standing on soil during the rotation of the boom, *International Journal of Mechanical Sciences,* 40 (6) (1998) 557-574.

[15] Z. Towarek, The function of the rheological soil strain under the foot supporting the crane, *Archive of Mechanical Engineering,* 46 (1) (1999) 5-18.

[16] A. Maczyński and S. Wojciech, The influence of selected parameters of model on crane dynamics, *VIII International Conference on the Theory of Machines and Mechanisms*, Liberec, September 5-7 (2000) 407-412.

[17] A. Maczyński, The influence of crane support flexibility on load motion, *4th EUROMECH Solid Mechanics Conference, Book of abstracts II,* General sessions, Metz, France, June 26-30 (2000) 519.

[18] T. Paszkiewicz, M. Osiński and S. Wojciech, Dynamic analysis of an offshore crane on offshore installations, *4th International Offshore Cranes Conference,* Stavanger, Norway, April 26-28 (1999) 2-38.

[19] W. Sochacki, The dynamic stability of a laboratory model of a truck crane, *Thin-Walled Structures,* 45 (2007) 927-930.

[20] A. Maczyński and S. Wojciech, Dynamics of a mobile crane and optimization of the slewing motion of its upper structure, *Nonlinear Dynamics,* 32 (3) (2003) 259-290.

[21] R. Mijailović, Modelling the dynamic behaviour of the truck-crane, *Transport,* 26 (4) (2011) 410-417.

[22] D. S. Han, S. W. Yoo, H. S. Yoon, M. H. Kim, S. H. Kim and J. M. Lee, Coupling analysis of finite element and finite volume method for the design and construction of FPSO crane, *Automation in Construction,* 20 (2011) 368-379.

[23] B. Jerman, P. Podrzaj and J. Kramar, An investigation of slewing-crane dynamics during slewing motion — development and verification of a mathematical model, *International Journal of Mechanical Sciences,* 46 (2004) 729-750.

[24] D. Kovaćević, I. Budak, A. Antić, A. Nagode and B. Kosec, FEM modeling and analysis in prevention of the waterway dredgers crane serviceability failure, *Engineering Failure Analysis,* 28 (2013) 328-339.

[25] D. Kovaćević, M. Soković, I. Budak, A. Antić and B. Kosec, Optimal finite elements method (FEM) model for the jib structure of a waterway dredger, *Metalurgija,* 51 (2012) 113-116.

[26] H. Schaub, Rate-based ship-mounted crane payload pendulation control system, *Control Engineering Practice,* 16 (2008) 132-145.

[27] B. Jerman and J. Kramar, Study of the horizontal inertial forces acting on the suspended load of slewing cranes, *International Journal of Mechanical Sciences,* 50 (2008) 490-500.

[28] R. M. Ghigliazza and P. Holmes, On the dynamics of cranes, or spherical pendula with moving supports, *International Journal of Non-Linear Mechanics,* 37 (2002) 1211-1221.

[29] K. Ellermann, E. Kreuzer and M. Markiewicz, Nonlinear dynamics of floating cranes, *Nonlinear Dynamics,* 27 (2002) 107-183.

[30] K. Ellermann and E. Kreuzer, Nonlinear dynamics in the motion of floating cranes, *Multibody System Dynamics,* 9 (2003) 377-387.

[31] H. Arayaa, M. Kakuzena, H. Kinugawab and T. Arai, Level luffing control system for crawler cranes, *Automation in Construction,* 13 (2004) 689-697.

[32] J. Neupert, E. Arnold, K. Schneider and O. Sawodny, Tracking and anti-sway control for boom cranes, *Control Engineering Practice,* 18 (2010) 31-44.

[33] N. Uchiyama, Robust control of rotary crane by partial-state feedback with integrator, *Mechatronics,* 19 (2009) 1294-1302.

[34] A. Trąbka, The choice of simplifications in development of numerical models of cranes with use of the finite element method (in Polish), *Teoria maszyn i mechanizmów - Mono-*

grafie, Wyd. AGH, Kraków, 2 (2004) 91-96.
[35] *ANSYS Help System* (2008).
[36] O. C. Zienkiewicz, *The Finite Element Method,* McGraw-Hill Company, London (1977).
[37] K. J. Bathe, *Finite Element Procedures in Engineering Analysis,* Prentice-Hall, Englewood Cliffs (1982).
[38] E. Sosna, *Influence of Flexibility of Support System on Dynamics of the Telescopic Mobile Crane* (in Polish), Praca doktorska, Politechnika Łódzka (1984).
[39] M. Trombski (Ed.), *Report on the implementation of subject no. 03.23.01: Optimization of support system of a truck crane as a member of the automatic control system of working movements, stage I, within the Polish Central Research Program 02.05* (in Polish), Instytut Mechaniczno - Konstrukcyjny Filii Politechniki Łódzkiej w Bielsku - Białej (1987).
[40] W. Jedliński (Ed.), *The dynamics of actuators of working machines including the control on the example of a telescopic crane, stages: I, II, III, IV, V, Implementation - Results - Conclusions, within the Polish Central Research Program 02.05, subject no. 03.13.01* (in Polish), Wydawnictwo Politechniki Warszawskiej (1990).
[41] T. J. R. Hughes, Numerical implementation of constitutive models: Rate-independent deviatoric plasticity, S. Nemat-Nasser, R. J. Asaro and G. A. Hegemier (Eds.), *Theoretical Foundation for Large-Scale Computations for Nonlinear Material Behavior,* Martinus Nijhoff Publishers, Dordrecht, The Netherlands (1984) 29-57.
[42] G. Strang, *Introduction to linear algebra,* Wellesley-Cambridge Press, Wellesley Massachusetts (2003).
[43] J. Argyris, An excursion into large rotations, *Computer Methods in Applied Mechanics and Engineering,* 32 (1982) 85-155.
[44] F. Minghini, Modeling of FRP pultruded structures using locking-free finite elements, *Ph.D. Thesis*, Università degli Studi di Ferrara (2008).
[45] C. C. Rankin and F. A. Brogan, An element independent corotational procedure for the treatment of large rotations, *Journal of Pressure Vessel Technology,* 108 (1986) 165-174.

Appendix

A.1 Description of the large strains analysis method

Some components of cranes (e.g. telescopic boom members, outriggers) under load are subject to such a large deformations that their shape change affects the location of the components associated with them. The above mentioned influence should be taken into account in calculations when the deformations exceeds a few percent (usually are $\geq 5\%$).

The large strains analysis method, used in this paper, is presented below. Explanations of the polar decomposition method and the midpoint method, are also included.

Consider the two configurations of a body, e.g. structural component of a crane, before and after deformation (Fig. A.1). Suppose a material particle A in a reference configuration

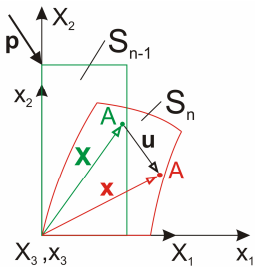

Fig. A.1. Position vectors and deformation of a body.

S_{n-1} (corresponding to time t_{n-1}) is defined by the vector **X**, and after applying a load vector **p**, due to the change of the configuration to S_n (corresponding to time t_n), its position is defined by the vector **x**. The position vector **x** is given by:

$$\mathbf{x} = \mathbf{X} + \mathbf{u} \tag{A.1}$$

where **u** is the displacement vector determined from Eq. (3).

In mathematical terms deformations describes the so-called deformation gradient tensor **F** :

$$\mathbf{F} = \frac{\partial \mathbf{x}}{\partial \mathbf{X}} = \begin{bmatrix} \partial x_1/\partial X_1 & \partial x_1/\partial X_2 & \partial x_1/\partial X_3 \\ \partial x_2/\partial X_1 & \partial x_2/\partial X_2 & \partial x_2/\partial X_3 \\ \partial x_3/\partial X_1 & \partial x_3/\partial X_2 & \partial x_3/\partial X_3 \end{bmatrix}. \tag{A.2}$$

The components of tensor **F** can be calculated based on the vector **u** :

$$\mathbf{F} = \frac{\partial(\mathbf{X}+\mathbf{u})}{\partial \mathbf{X}} = \frac{\partial \mathbf{X}}{\partial \mathbf{X}} + \frac{\partial \mathbf{u}}{\partial \mathbf{X}} = \mathbf{I} + \frac{\partial \mathbf{u}}{\partial \mathbf{X}} \tag{A.3}$$

where **I** is the 3x3 identity matrix.

The tensor **F** includes the information about all components of the deformation process, i.e. the shape change, the volume change and the rotation. In order to separate from the tensor **F** the information about the shape changes, this tensor should be subjected to the so-called polar decomposition. *The polar decomposition theorem* is based on a division of the deformation process into two stages, i.e. the step of changing the shape and the step of rotation, wherein their order may be arbitrary:

$$\mathbf{F} = \mathbf{R} \cdot \mathbf{U} \tag{A.4}$$

$$\mathbf{F} = \mathbf{V} \cdot \mathbf{R} \tag{A.5}$$

where **R** is the rotation matrix (with the following properties: $\mathbf{R}^{\mathrm{T}} \cdot \mathbf{R} = \mathbf{R}^{-1} \cdot \mathbf{R} = \mathbf{I}$), **U** is the right stretch (shape change) matrix determined with respect to the reference configuration of the body (this matrix is symmetric, so $\mathbf{U} = \mathbf{U}^T$ and $\mathbf{U}^T \cdot \mathbf{U} = \mathbf{U} \cdot \mathbf{U}$), **V** is the left stretch matrix.

The real strain (also called *Hencky strain* or *logarithmic strain*) in advanced materials models for one-dimensional

(1D) deformations is defined as:

$$\varepsilon = \ln\left(\frac{l}{L}\right) \tag{A.6}$$

where l is the final length of a material fiber, L is the initial length of the fiber.

Taking into account that the individual elements of the matrix $\mathbf{U}$ contain information about the component stretches of a material particle, the real strain tensor for a three-dimensional (3D) system may be determined as:

$$\boldsymbol{\varepsilon} = \ln \mathbf{U} . \tag{A.7}$$

In this paper, the approximate 2nd order accurate calculations of the real strain tensor $\boldsymbol{\varepsilon}$ (proposed by Hughes [41]), have been used. These calculations are based on the incremental procedure, because the logarithmic strain provides the correct measure of the final strain when deformation takes place in a series of increments. The basis of this method is Eq. (A.8) from which the increase of a so-called pure (i.e. devoid of a rotational component) strain $\Delta\boldsymbol{\varepsilon}_n$, in the n-th time step is calculated.

$$\Delta\boldsymbol{\varepsilon}_n = \mathbf{R}^T_{n-1/2} \cdot \Delta\boldsymbol{\varepsilon}^R_n \cdot \mathbf{R}_{n-1/2} \tag{A.8}$$

where $\Delta\boldsymbol{\varepsilon}^R_n$ is the tensor of the strain increment caused by the rotation in the n-th time step.

In order to improve the approximation accuracy in the calculations of Eq. (A.8) right side components, the so-called *midpoint method* has been applied. This method consists in the fact that the values in the subsequent time steps are determined on the basis of the values approximated at the points located midway between the actual value and the one that precedes it directly. Based on the above method the midpoint displacement vector $\mathbf{u}_{n-1/2}$ is determined first:

$$\mathbf{u}_{n-1/2} = \frac{1}{2} \cdot \left(\mathbf{u}_n + \mathbf{u}_{n-1}\right) \tag{A.9}$$

where $\mathbf{u}_n$ is the displacement vector for n-th step, $\mathbf{u}_{n-1}$ is the displacement vector for n-1 step.

Then the midpoint tensor $\mathbf{F}_{n-1/2}$ (based on Eq. (A.3)) and the midpoint matrix $\mathbf{R}_{n-1/2}$ (based on Eq. (A.4)), are determined:

$$\mathbf{F}_{n-1/2} = \mathbf{I} + \frac{\partial \mathbf{u}_{n-1/2}}{\partial \mathbf{X}} \tag{A.10}$$

$$\mathbf{R}_{n-1/2} = \mathbf{F}_{n-1/2} \cdot \mathbf{U}^{-1}_{n-1/2} . \tag{A.11}$$

In order to determine the shape change matrix for the midpoint configuration $\mathbf{U}_{n-1/2}$, first the tensor $\mathbf{F}_{n-1/2}$ is premultiplied by its transpose:

$$\begin{aligned}
&\mathbf{F}^T_{n-1/2} \cdot \mathbf{F}_{n-1/2} = \\
&= \left(\mathbf{R}_{n-1/2} \cdot \mathbf{U}_{n-1/2}\right)^T \cdot \left(\mathbf{R}_{n-1/2} \cdot \mathbf{U}_{n-1/2}\right) = \\
&= \mathbf{U}^T_{n-1/2} \cdot \mathbf{R}^T_{n-1/2} \cdot \mathbf{R}_{n-1/2} \cdot \mathbf{U}_{n-1/2} = \\
&= \mathbf{U}^T_{n-1/2} \cdot \mathbf{U}_{n-1/2} = \mathbf{U}_{n-1/2} \cdot \mathbf{U}_{n-1/2} = \mathbf{U}^2_{n-1/2} .
\end{aligned} \tag{A.12}$$

Then, in order to calculate the square roots of Eq. (A.12) the coordinate system is transformed to the orientation at which $\mathbf{U}^T_{n-1/2} \cdot \mathbf{U}_{n-1/2}$ has the form of a diagonal matrix $\left(\mathbf{U}^2_{n-1/2}\right)_{diag}$. Since the elements of the transformation matrix $\mathbf{Q}_{n-1/2}$ are eigenvectors (principal directions) $\mathbf{v}_i$ of the matrix $\mathbf{U}^2_{n-1/2}$, and the elements of the diagonal matrix $\left(\mathbf{U}^2_{n-1/2}\right)_{diag}$ are eigenvalues (principal stretches) λ_i of this matrix, a spectral decomposition of the matrix $\mathbf{U}^2_{n-1/2}$ is performed. This is done by calculation of $\mathbf{v}_i$ and λ_i from Eq. (A.13) (detailed description can be found in chapter 6 of Ref. [42]).

$$\left(\mathbf{U}^2_{n-1/2} - \lambda \cdot \mathbf{I}\right) \cdot \mathbf{v} = 0 . \tag{A.13}$$

In the next step $\mathbf{U}_{n-1/2}$ in the original coordinate system is calculated:

$$\mathbf{U}_{n-1/2} = \mathbf{Q}^T_{n-1/2} \cdot \sqrt{\left(\mathbf{U}^2_{n-1/2}\right)_{diag}} \cdot \mathbf{Q}_{n-1/2} \tag{A.14}$$

where: $\mathbf{Q}_{n-1/2} = \begin{bmatrix} \mathbf{v}_1 & \mathbf{v}_2 & \mathbf{v}_3 \end{bmatrix}$ (A.15)

and $\left(\mathbf{U}^2_{n-1/2}\right)_{diag} = \begin{bmatrix} \lambda_1 & 0 & 0 \\ 0 & \lambda_2 & 0 \\ 0 & 0 & \lambda_3 \end{bmatrix}$. (A.16)

Then the inverse of $\mathbf{U}_{n-1/2}$ is determined, and finally $\mathbf{R}_{n-1/2}$ from Eq. (A.11) is calculated.

The second component of the right side of Eq. (A.8), i.e. the tensor $\Delta\boldsymbol{\varepsilon}^R_n$ is determined on the basis of the corresponding vector $\Delta\mathbf{e}^R_n$ obtained from the equation:

$$\Delta\mathbf{e}^R_n = \mathbf{B}_{n-1/2} \cdot \Delta\mathbf{u}_n \tag{A.17}$$

where $\mathbf{B}_{n-1/2}$ is the strain–displacement relationship evaluated at the midpoint geometry (see Eq. (A.18)), $\Delta\mathbf{u}_n$ is the displacement increment vector ($\Delta\mathbf{u}_n = \mathbf{u}_n - \mathbf{u}_{n-1}$).

$$\begin{aligned}
&\mathbf{B}^T_{n-1/2} = \\
&= \begin{bmatrix}
\dfrac{\partial N}{\partial x_{1;n-1/2}} & 0 & 0 & \dfrac{\partial N}{\partial x_{2;n-1/2}} & 0 & \dfrac{\partial N}{\partial x_{3;n-1/2}} \\
0 & \dfrac{\partial N}{\partial x_{2;n-1/2}} & 0 & \dfrac{\partial N}{\partial x_{1;n-1/2}} & \dfrac{\partial N}{\partial x_{3;n-1/2}} & 0 \\
0 & 0 & \dfrac{\partial N}{\partial x_{3;n-1/2}} & 0 & \dfrac{\partial N}{\partial x_{2;n-1/2}} & \dfrac{\partial N}{\partial x_{1;n-1/2}}
\end{bmatrix}
\end{aligned} \tag{A.18}$$

where N is the shape function depending on the type of finite element, $x_{j;n-1/2}=\frac{1}{2}\cdot\left(x_{j;n}+x_{j;n-1}\right)$ is the midpoint configuration of the body and $j=1,2,3$.

Since $\Delta\mathbf{e}_n^R=\left[\Delta\varepsilon_{11}\quad\Delta\varepsilon_{22}\quad\Delta\varepsilon_{33}\quad\Delta\varepsilon_{12}\quad\Delta\varepsilon_{23}\quad\Delta\varepsilon_{31}\right]^T$, due to the symmetry we obtain:

$$\Delta\boldsymbol{\varepsilon}_n^R=\begin{bmatrix}\Delta\varepsilon_{11} & \Delta\varepsilon_{12} & \Delta\varepsilon_{13}\\ \Delta\varepsilon_{21} & \Delta\varepsilon_{22} & \Delta\varepsilon_{23}\\ \Delta\varepsilon_{31} & \Delta\varepsilon_{32} & \Delta\varepsilon_{33}\end{bmatrix}. \tag{A.19}$$

Tensor $\Delta\boldsymbol{\varepsilon}_n^R$ inserted into Eq. (A.8) allows the calculation of the pure strain increment $\Delta\boldsymbol{\varepsilon}_n$ in the n-th time step. In turn, $\Delta\boldsymbol{\varepsilon}_n$ added to the previous strain $\boldsymbol{\varepsilon}_{n-1}$ allows determining the real strain in the n-th time step:

$$\boldsymbol{\varepsilon}_n=\boldsymbol{\varepsilon}_{n-1}+\Delta\boldsymbol{\varepsilon}_n\,. \tag{A.20}$$

A.2 Description of the relationship between the transformation matrix and the rotational pseudovector in a large rotation analysis

Rotation in the 3D may be described by the nine direction cosines (Eq. (A.21)).

$$R=\begin{bmatrix}\cos\theta_{x_1X_1} & \cos\theta_{x_2X_1} & \cos\theta_{x_3X_1}\\ \cos\theta_{x_1X_2} & \cos\theta_{x_2X_2} & \cos\theta_{x_3X_2}\\ \cos\theta_{x_1X_3} & \cos\theta_{x_2X_3} & \cos\theta_{x_3X_3}\end{bmatrix} \tag{A.21}$$

where $\theta_{x_1X_1}$ is the angle that the rotated x_1 axis makes with the fixed X_1 axis, $\theta_{x_2X_1}$ is the angle that the rotated x_2 axis makes with the fixed X_1 axis, and so on; $\{X_1,X_2,X_3\}$ is a fixed orthogonal coordinate triad, $\{x_1,x_2,x_3\}$ is an orthogonal triad that rotates, and is initially coincident with the previous one.

One of the Euler's theorem states that any rotation may be specified in a simplified form by an axis and an angle of rotation. According to this theorem, Argyris decided to describe a large rotation in space by a vector defined as $\boldsymbol{\theta}=\theta\cdot\mathbf{e}$ [43]. He named this vector "*rotational pseudovector*". Accordingly to the definition, pseudovector has a length equal to a rotation angle θ and is directed as a unit vector $\mathbf{e}$, which defines an axis of rotation and passes through a fixed point placed at the origin of global coordinates (Fig. A.2).

Pseudovector has three Cartesian components: $\theta_1,\theta_2,\theta_3$, and its length (the norm) is: $\theta=\left(\theta_1^2+\theta_2^2+\theta_3^2\right)^{\frac{1}{2}}$. So defined pseudovector fully describes 3D rotations using only three parameters instead of the nine employed in the matrix representation.

Based on the $\boldsymbol{\theta}$ definition, Eq. (A.22) describing a transformation of a vector $\mathbf{z}_0$ into a vector $\mathbf{z}$ (Fig. A.2) by means of a generic large rotation is established.

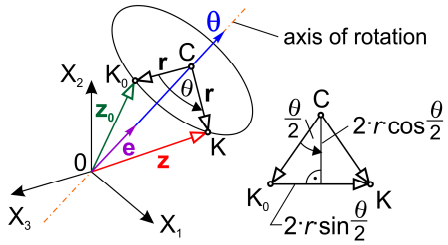

Fig. A.2. Transformation of vector $\mathbf{z}_0$ into vector $\mathbf{z}$ by means of a generic large rotation with pseudovector $\boldsymbol{\theta}$.

$$\mathbf{z}=\mathbf{T}_{\boldsymbol{\theta}}\cdot\mathbf{z}_0 \tag{A.22}$$

where $\mathbf{T}_{\boldsymbol{\theta}}$ is a transformation matrix known as the Rodriguez formula:

$$\mathbf{T}_{\boldsymbol{\theta}}=\mathbf{I}+\frac{\sin\theta}{\theta}\cdot\mathbf{S}(\boldsymbol{\theta})+\frac{1}{2}\cdot\left(\frac{\sin\theta/2}{\theta/2}\right)^2\cdot\mathbf{S}(\boldsymbol{\theta})^2 \tag{A.23}$$

$$\mathbf{S}(\boldsymbol{\theta})=\begin{bmatrix}0 & -\theta_3 & \theta_2\\ \theta_3 & 0 & -\theta_1\\ -\theta_2 & \theta_1 & 0\end{bmatrix}. \tag{A.24}$$

Eq. (A.23) is derived based on the vector relations visible in Fig. A.2 (for detailed description of this derivation see chapter 3.3 in Ref. [44]).

Then adopting *normalisation* of Rankin and Brogan [45], i.e. scaling components e_1,e_2,e_3 of the vector $\mathbf{e}$ by a new quantity (the norm) ω instead of θ, a new rotational pseudovector $\overline{\boldsymbol{\omega}}$ is written as:

$$\overline{\boldsymbol{\omega}}=\left[\omega_1\quad\omega_2\quad\omega_3\right]^T=\omega\cdot\mathbf{e} \tag{A.25}$$

where $\omega_1,\omega_2,\omega_3$ are the normalised pseudovector components, ω is the length of the normalised pseudovector.

Since in general the norm of $\mathbf{e}$ is a function of θ, following Rankin and Brogan the relationship between ω and θ is adopted as:

$$\omega=2\cdot\sin\frac{\theta}{2}\,. \tag{A.26}$$

Thus:

$$\overline{\boldsymbol{\omega}}=2\cdot\sin\frac{\theta}{2}\cdot\mathbf{e}\,. \tag{A.27}$$

Then Eq. (A.27) is inserted into Eq. (A.23). Thus the transformation matrix $\mathbf{T}_{\boldsymbol{\omega}}$ associated with pseudovector $\overline{\boldsymbol{\omega}}$ is obtained in the form:

$$\mathbf{T}_{\boldsymbol{\omega}}=\mathbf{I}+\sqrt{1-\left(\frac{\omega}{2}\right)^2}\cdot\boldsymbol{\Omega}+\frac{1}{2}\cdot\boldsymbol{\Omega}^2 \tag{A.28}$$

where $\mathbf{\Omega}$ is the skew-symmetric matrix representation of $\overline{\boldsymbol{\omega}}$.

$$\mathbf{\Omega} = \begin{bmatrix} 0 & -\omega_3 & \omega_2 \\ \omega_3 & 0 & -\omega_1 \\ -\omega_2 & \omega_1 & 0 \end{bmatrix}. \tag{A.29}$$

The transformation matrix enables monitoring the rotation of finite elements with respect to the global Cartesian coordinate system. Obtained this way information allow to extract the deformational displacement from the total element displacement, and then allow to compute the element stiffness matrix as well as the strains and stresses.

Arkadiusz Trąbka received his master degree in Mechanical Engineering from Bielsko-Biala Branch of Lodz University of Technology. He received his doctor degree in 2003 from the Faculty of Mechanical Engineering and Computer Science at the University of Bielsko-Biala. His research interests include kinematics and dynamics of construction machinery, FEM and multibody analysis.